EPR, ENDOR, and HYSCORE Study of the Structure and the Stability of Vanadyl−Porphyrin Complexes Encapsulated in Silica: Potential Paramagnetic Biomarkers for the Origin of Life

Didier Gourier,*,† Olivier Delpoux,† Audrey Bonduelle,† Laurent Binet,† Ilaria Ciofini,‡ and Hervé Vezin§

Laboratoire de Chimie de la Matière Condensée de Paris, Ecole Nationale Supérieure de Chimie de Paris (Chimie ParisTech) and Université Pierre et Marie Curie, UMR-CNRS 7574, 11 rue Pierre et Marie Curie, 75231 Paris cedex 05, France, Laboratoire d'Electrochimie, Chimie des Interfaces et Modélisation pour l'Energie, Ecole Nationale Supérieure de Chimie de Paris (Chimie ParisTech), UMR-CNRS 7575, 11 rue Pierre et Marie Curie, 75231 Paris cedex 05, France, and Laboratoire de Spectrochimie Infrarouge et Raman, Université des Sciences et Technologes de Lille, UMR-CNRS 8516, 59655 Villeneuve d'Ascq, France

Received: December 11, 2009; Revised Manuscript Received: February 8, 2010

The possibility of using vanadyl ions as paramagnetic biomarkers for the identification of traces of primitive life fossilized in silica rocks is studied by cw-EPR, ENDOR, HYSCORE, and DFT calculations. It is well-known that porphyrins, which are common to all living organisms, form vanadyl−porphyrin complexes in sediments deposited in oceans. However, the stability of these complexes over a very long time (more than 3 billion years) is not known. By encapsulating vanadyl−porphyrin complexes in silica synthesized by a sol−gel method to mimic SiO_2 sediments, we studied the structure and stability of these complexes upon step heating treatments by monitoring the evolution of the *g* factor and of the hyperfine interactions with ^{51}V, ^{1}H, ^{14}N, ^{13}C, and ^{29}Si nuclei. It is found that vanadyl−porphyrin complexes are progressively transformed into oxygenated vanadyl complexes by transfer of the VO^{2+} ion from the porphyrin ring to the mineral matrix. The organic component is transformed into carbonaceous matter which contains paramagnetic centers ($IOM^{\bullet}$ centers). To test the validity of this approach, we studied by EPR a 3490 million years old chert (polycrystalline SiO_2 rock) containing some of the oldest putative traces of life. This rock contains oxygenated vanadyl complexes and $IOM^{\bullet}$ centers very similar to those found in the synthetic analogues.

Introduction

The identification of physicochemical signatures of the oldest fossilized life on Earth or on Mars is a challenging issue to determine with regards to when, where, and how the first microorganisms appeared.[1] The oldest (∼3500 million years (Myr)) and best preserved putative traces of life are found in the form of carbonaceous microstructures embedded in cherts, which are polycrystalline SiO_2 rocks originating from silica sediments deposited on the floor of primitive seas. Their attribution to fossilized bacteria was initially proposed on the basis of morphological observations[2] and of laser Raman microspectroscopy for the identification of amorphous carbon material.[3] However, Raman spectroscopy alone cannot assess the biologic origin of these microstructures,[4] and abiotic processes such as Fischer−Tropsch reactions or thermal decomposition of carbonates are able to give the same types of carbonaceous material with the same Raman signature.[5–7] Also, carbon isotope fractionation has often been considered as a criterion for the biologic origin of the carbonaceous matter in the oldest rocks.[8,9] Unfortunately, abiotic processes can also lead to the same carbon isotope composition.[10–12] Thus, there is still a lack of consensus in the scientific community on which observables could be considered as reliable biosignatures, and at present, there are no physicochemical markers which can help to determine the origin of ancient carbonaceous matter. Therefore, the determination of stable and reliable biosignatures is a fundamental issue in the search for traces of primitive life on Earth, and also on Mars, which offers conditions of habitability similar to that of early Earth at the same epoch.[1]

Even when the biogenic origin of a fossilized carbonaceous matter is ascertained, it must be checked that it is indigenous to, and synchronous with, the host rock and not the result of a recent biological contamination. As an emblematic example, the polycyclic aromatic compounds and the related organic matter found in the famous Martian meteorite ALH84001[13] were found to be recent and of terrestrial origin.[14,15] An undisputable molecular biomarker of primitive life should exhibit several characteristics: (i) it must be common to all known living organisms, especially prokaryotes (bacteria, archea) and cannot be synthesized by abiotic processes existing in primitive geological environments; (ii) it must be demonstrated that it is synchronous with the host rock and does not originate from more recent biological contamination (water circulation, endolithic bacteria, anthropic contamination from chemical operations, etc.); (iii) it must be detectable at very small concentration, preferably without chemical sample preparation, to avoid anthropic contamination and to be compatible with Mars sample studies.

* To whom correspondence should be addressed. E-mail: didier-gourier@chimie-paristech.fr.

† Laboratoire de Chimie de la Matière Condensée de Paris, Ecole Nationale Supérieure de Chimie de Paris (Chimie ParisTech) and Université Pierre et Marie Curie.

‡ Laboratoire d'Electrochimie, Chimie des Interfaces et Modélisation pour l'Energie, Ecole Nationale Supérieure de Chimie de Paris (Chimie ParisTech).

§ Université des Sciences et Technologes de Lille.

10.1021/jp911728e
Published on Web 02/22/2010

Metalloporphyrins, and more particularly vanadyl (VO^{2+}) porphyrins (VO−P), satisfy all of these criteria. Porphyrins are present in all living systems, even the most primitive ones. Porphyrin-based molecules are involved in different energy-producing mechanisms of bacteria and archea, depending on the type of metal associated to the porphyrin. For example, anaerobic and aerobic respirations involve cytochromes, where porphyrins are complexed with Fe^{2+}, methanogenesis and acetogenesis involve complexation with Ni^{2+} or Co^{2+}, and oxygenic and anoxygenic photosyntheses involve complexation with Mg^{2+} (bacteriochlorophylls).[16] The post mortem degradation mechanisms of the biological matter in water environment are complex, and some molecules, among which are porphyrins, are stable over several millions of years in geological material. Metal ions of the porphyrins are progressively replaced by vanadyl, giving very stable VO−P complexes. This is the reason why VO−P's are universally found within biogenic terrestrial carbonaceous materials such as petroleum, bitumen, and coals, which triggered off the organic geochemistry.[17–20] The exceptional stability of geoporphyrins explains why they are found in a variety of geological formations.[21,22] With vanadyl−porphyrin geomarkers being unquestionably of biologic origin and porphyrins being present in all living systems, these complexes should constitute ideal biomarkers for the search of traces of primitive life in the most ancient geological materials (Archean period, older than 2500 Myr) and probably in some Martian sedimentary rocks (Noachian period, older than 3500 Myr).[23] Thus VO−Ps satisfy both criteria (i) and (ii), as complexation with VO^{2+} occurs only in water environment, upon reduction of soluble vanadate ions. Later contamination of the rock by endolithic bacteria or by ambient bacteria, where porphyrins conserve their own metal ions, can be easily distinguished from porphyrins synchronous to the formation of the sedimentary rocks, which form complexes with VO^{2+}.

VO^{2+} is paramagnetic (vanadium is in the V(IV) state with a $3d^1$ electron configuration), so that vanadyl−porphyrins in petroleum, coals, and rocks are easily detected with high sensitivity (criterion (iii)) by electron paramagnetic resonance (EPR) spectroscopy.[24,25] However, it is not known if the stability of such vanadyl−porphyrins is sufficiently high to protect them from complete destruction in rocks as old as 3.5−3.8 Ga, which contain some of the oldest putative traces of life and which are often deeply transformed by the effect of temperature and pressure.[26] It is thus of fundamental interest to identify the degradation process and the degradation products of vanadyl−porphyrins in a mineral environment. Once identified, these degradation products could be considered as second-order biomarkers of primitive life.

The best preservation of carbonaceous matter older than about 2500 Myr (Archean period) is found in cherts, where the compact microcrystalline SiO_2 matrix with minor secondary mineral phases protects the carbonaceous matter from migration and oxidation. Some of the oldest (3490 Myr) traces of life on Earth are found in chert horizons of the lower Warrawoona group in Western Australia. However, the biogenic origin of these carbonaceous microstructures is highly debated,[27–29] and similar morphological structures can be formed through abiotic conditions.[4–7] For these reasons, the presence of carbonaceous microstructures in a very ancient silica rock does not constitute an indisputable proof of the presence of fossilized microorganisms. Cherts from the Warrawoona group contain a few tenths of a ppm of vanadium originating from hydrothermal emissions on the floor of the primitive ocean.[30] This concentration is sufficient for detection by EPR if a significant part of vanadium is in the V(IV) state. If bacteria, and thus porphyrins, were present in ancient sea, we would expect VO−P complexes to have been formed and preserved or transformed in the chert.

In order to analyze the degradation products of vanadyl−porphyrins in cherts, we study in this work the electronic structure and the thermal stability of vanadyl−porphyrin in silica by using various EPR methods assisted by DFT calculations. Vanadyl tetraphenylporphyrin (VOTPP) complexes are encapsulated in a silica matrix synthesized in an aqueous way by a sol−gel method, in conditions compatible with those prevailing in primitive oceans. The integrity of the complex, its electronic structure, and its thermal stability are studied by monitoring the g factor and the ^{51}V hyperfine (hf) interaction of VO^{2+} and also the hf interactions with nuclei of the porphyrin and the mineral matrix. Electron nuclear double resonance (ENDOR)[31] is used for ^{1}H nuclei, and HYperfine Sublevel CORrelation (HYSCORE) spectroscopy is used for ^{14}N, ^{13}C, and ^{29}Si.[32,33] To test the validity of our experimental approach and the relevance of VO^{2+} as biomarkers, we analyzed, without any sample preparation, a chert containing the oldest (3490 Myr) putative traces of life in the form of carbonaceous microstructures. Molecular markers of primitive life were recently found in the carbonaceous matter extracted from this chert.[29] Only continuous wave (cw)-EPR can be used in that case because the poor sensitivity resulting from the very low vanadium content of the sample (a few tenth of a ppm) precludes the use of more sophisticated EPR techniques such as ENDOR and HYSCORE.

Samples and Methods

Encapsulation of VOTPP in Silica. Three types of samples were synthesized to study the thermal stability of vanadyl−porphyrins, (i) silica embedding VOTPP alone, (ii) silica embedding VOTPP and a protein (bovin serum albumin, BSA) to mimick the presence of biomacromolecules, and (iii) silica with BSA alone to discriminate the degradation of VOTPP from that of biomolecules. Silica was synthesized by a sol−gel method based on tetramethyl siloxane (TMOS) precursors.[34] The resulting gel was doped with VOTPP by impregnation with a chloroform solution of a metal complex. A basic catalyst was chosen to synthesize VOTPP-doped silica (hereafter referred to as VOTPP−SiO_2) since it ensures the stability of VOTPP while this complex is degraded under acidic conditions. The following process was used. TMOS (2 g) was mixed with CH_3OH (0.84 g) and water at pH 10 (1 mL of NaOH, 10^{-4} M). Gelation occurred within 1 h. Next, the gels were aged for one week at room temperature in a closed vessel and rinsed with a 50:50 water−methanol solution for 20 min, pure methanol for 20 min, a 50:50 methanol−chloroform mixture for 20 min, and pure chloroform for 20 min. A solution of VOTPP in chloroform (10^{-3} M) was next added to the gel (volumic ratio $V_{solution}/V_{gel} = 1$). After 20 min, the gel took a uniform red color, indicating that VOTPP was homogeneously dispersed in the gel matrix. The solution was eliminated, and the gel was rinsed with pure chloroform to eliminate surface VOTPP. Dry gels were obtained by drying the impregnated gels in open air at room temperature. After this treatment, the EPR at room temperature (not shown) exhibited a typical "powder" line shape of vanadyl complex.[35] However the lines were broadened by the rapid molecular tumbling effect resulting from the presence of residual solvent molecules.

The synthesis of silica containing both VOTPP and BSA (hereafter referred to as VOTPP/BSA−SiO_2) was performed with a mixed catalyst using a phosphate buffer; 1 mL of 10^{-1} M HCl was added to a solution containing 2 g of TMOS and

0.84 g of CH_3OH. Next, the solution was mixed for 10 min for complete hydrolysis. After addition of 1 mL of a phosphate buffer with 1 mg of BSA, the gel consolidated in a few seconds. Afterward, it was aged for 2 days to prevent the gel from breaking up during impregnation. The gel was rinsed with water−methanol (50:50), methanol, methanol−chloroform (50:50), and chloroform before impregnation. Each solvent was kept in contact with the gel for 20 min ($V_{solvent}/V_{gel} = 1$) and was removed each time before another rinsing. Finally, the porphyrin solution was added until the gel became homogenously red. Another rinsing was necessary to remove the porphyrins from the outer surfaces. A sample containing only BSA was also synthesized (hereafter referred to as BSA−SiO_2) in order to separate clearly the degradation products of VOTPP and BSA in the HYSCORE spectra.

In all cases, the solvent was eliminated by inserting the samples in EPR tubes, pumping and sealing them under vacuum, and treating them for 30 min at 120 °C. After this treatment, the EPR spectra exhibited a well-resolved powder hyperfine pattern of VOTPP with narrow lines and no EPR signal when only BSA was encapsulated. Thermal aging of VOTPP−SiO_2, VOTPP/BSA−SiO_2, and BSA−SiO_2 samples was carried out in vacuum by isochronal step heating treatments of the sealed tubes for short times (15 min) by steps of 50 °C and recording the EPR spectrum at room temperature after each thermal step.

The effect of confinement in the silica matrix was studied by comparing the EPR and ENDOR spectra of VOTPP encapsulated in silica with those of a frozen VOTPP solution (5×10^{-3} M) in $CHCl_3$.

Chert Samples. The 3490 Myr old chert studied in this work comes from the Dresser formation, Warrawoona Group in Australia. The sample was selected for this study from a large collection of cherts on the basis of its isotopic composition,[36] the presence of carbonaceous microstructures interpreted as microfossils,[37,38] and the recent evidence of biomolecular markers of primitive life.[29] The samples (PPRG 006 from the Schopf collection) are only slightly metamorphosed by the effect of temperature and pressure. They were collected in the lower chert horizon of the Dresser Formation in the North Pole B Mine.[39] The chert consists dominantly of microcrystalline quartz, and X-ray diffraction only shows diffraction peaks of α-quartz, indicating that other minerals contribute to less than about 5% of the chert. Minority phases are observed by combining optical microscopy and micro-Raman spectroscopy, the most common phases being hematite (Fe_2O_3), barite ($BaSO_4$), and anatase (TiO_2). Other iron oxide and hydroxide phases were also observed. VO^{2+} in bulk rock was studied by EPR without sample preparation.

Electron Paramagnetic Resonance. CW-EPR spectra were recorded at the X band (9.5 GHz) with a Bruker ELEXSYS E500 spectrometer equipped with a high-sensitivity 4122SHQE/0111 microwave cavity and with a helium flow cryostat for low-temperature measurements. The hyperfine (hf) interactions A with ^{51}V nuclei ($I = 7/2$, 99.75% abundance) are given in cm^{-1}, as is usual for transition-metal complexes.[35] They are related to A and measured in magnetic field units (mT) by the following expression

$$A\ (cm^{-1}) = 4.66864 \times 10^{-4} \times g \times A\ (mT) \qquad (1)$$

The EPR spectra were simulated with the software WINSIMFONIA from Bruker Biospin for extraction of g factors and ^{51}V hf interaction parameters. The vanadyl concentrations were determined by comparing the EPR spectra (experimental or simulated) with that of a frozen solution of vanadyl acetylacetonate in chloroform. A calibration curve for spin concentration measurements was obtained with different concentrations of the reference. Measurements were performed at 10 K (samples and reference). Owing to the fact that VO^{2+} hf lines of the chert overlap with other EPR signals of the fossilized carbonaceous matter and the mineral matrix, spin concentrations were measured by comparing the amplitudes of the perpendicular component of the $m_I = -5/2$ hf line (see below), which is relatively intense and well-separated from other EPR lines.

Small hf interactions with neighboring nuclei (^1H, ^{14}N, ^{13}C, and ^{29}Si) of VOTPP are not resolved in the standard cw-EPR spectra. ^1H hf parameters were studied with continuous-wave ENDOR at 10 K with the Bruker ELEXSYS E500 EPR spectrometer equipped with an ENDOR TM_{110} cylindrical cavity. The radiofrequency (rf) field produced by a Wavetek 3000-446 synthesizer was amplified by a 100 W ENI 3100 L broad-band amplifier. Hyperfine interactions with ^{13}C, ^{14}N, and ^{29}Si nuclei were studied by pulsed EPR at 4 K with a Bruker ELEXSYS E580 spectrometer. A spin echo was generated by a series of $\pi/2$ and π microwave pulses ($\pi/2$ and π represent the rotation angles of the electron magnetization), with controlled time delays between pulses. By varying these time delays, the echo intensity exhibited modulations at the frequencies of the hf interactions. We used the pulse sequence $\pi/2-\tau-\pi/2-t_1-\pi-t_2-\pi/2-\tau-$echo (HYperfine Sublevel CORrelation Spectroscopy, HYSCORE), whereby an echo was generated at time τ after the last $\pi/2$ pulse, τ representing the delay between the first and second $\pi/2$ pulses. The echo intensity was measured at each t_1 and t_2 value, which were varied stepwise at constant τ. This two-dimensional set of echoes gave, after Fourier transform along t_1 and t_2, a two-dimensional HYSCORE spectrum.[32] The lengths of the $\pi/2$ and π pulses were 16 and 32 ns, respectively, and a delay of $\tau = 128$ ns between the first two $\pi/2$ pulses gave the best sensitivity and resolution for the detection of ^{14}N, ^{13}C, and ^{29}Si peaks. HYSCORE spectroscopy was also used to study the thermal stability of VOTPP encapsulated in silica by monitoring the evolution of ^{14}N, ^{13}C, and ^{29}Si interactions upon step heating treatments. HYSCORE spectra were recorded with 256×256 data points for both t_1 and t_2 time domains. Second-order polynomial background subtraction was performed to remove the unmodulated part of the echo. 2D-Fourier transformation of the spectra was performed using a Hamming apodization window function, and the magnitude was calculated. ENDOR and HYSCORE gave no exploitable results for vanadyl ions in natural samples because of their very low vanadium content (a few tenths of a ppm); therefore, only cw-EPR was used in this case.

Simulation of HYSCORE spectra was achieved using the EasySpin toolbox for Matlab.[40] The subroutine program was written using the density matrix formalism. The experimental values of τ and of the $\pi/2$ and π pulse lengths were also used in the simulation. The simulation of the spectra was achieved for the magnetic field settings $m_I = -7/2_{||}$ and $-3/2_{\perp}$ of the ^{51}V hyperfine pattern (see Figure 2) using sets of hyperfine and quadrupolar parameters for nitrogen and carbon atoms calculated with DFT methods. The simulated spectrum was obtained by Fourier transformation of the time domain signal using the Hamming apodization function. The axial peak due to the transfer of nuclear coherence to polarization was removed by setting the corresponding values to 0, preventing the use of the phase-cycling method and consequently speeding up the calculation of time domain spectra.

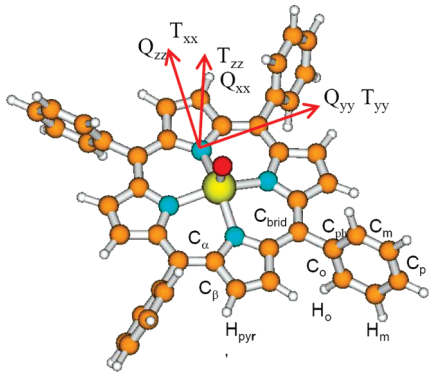

Figure 1. DFT-computed structure of VOTPP in the gas phase. Vanadium, carbon, oxygen, and nitrogen atoms are represented in yellow, orange, red, and blue, respectively. The different types of carbon and hydrogen atoms for which hyperfine parameters are computed are indicated. Arrows represent the tensor axes of the dipolar T and quadrupolar Q interactions of nitrogen nuclei.

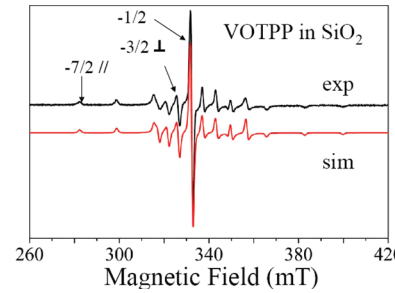

Figure 2. Experimental and simulated EPR spectra at room temperature of VO^{2+} in a VOTPP−SiO_2 sample. Microwave power: 1 mW; a pseudo-Voigt line shape was used for the simulation. This line shape is characterized by $x = 0.3$, defined as $(1 - x)L + xG$, where L and G are expressions of Lorentzian (L) and Gaussian (G) derivative functions, respectively. The spectra (not shown) obtained for VOTPP/BSA−SiO_2 samples are undistinguishable from those of VOTPP−SiO_2.

Computational Details. All calculations were performed within the unrestricted formalism, and spin contamination, monitored by the S^2 expectation value, was always found to be negligible. Structural optimizations were carried out at the DFT level using the Gaussian code.[41] A hybrid exchange correlation functional, hereafter PBE0, was used throughout.[42] It was preferred to other available hybrids due to its proven solid performances in the calculation of a wide variety of magnetic properties of metal complexes.[43–45] The PBE0 was derived from the PBE functional,[46] fixing the HF/DFT exchange ratio a priori to 1/4.[47] A double-ξ quality LANL2 basis[48] and the corresponding pseudopotential[49] were used for all atoms. The nature of the stationary points (i.e., minima) was determined by successive frequency calculations. No symmetry constraints were imposed, although an overall C_4 symmetry of the vanadyl complex was found. As a consequence, only symmetry-independent EPR parameters are given in the text. With optimized structures, both isotropic (a_{iso}) and dipolar (T) contributions to the hyperfine coupling tensor were computed at the PBE0 level using the Gaussian code and the EPR-II[50] all-electron basis for all atoms but vanadium, which was described using a Pople double-ζ valence plus polarization basis (6-31G(*)).[51] When referring to spin density, Mulliken spin distributions computed at this level of theory are discussed. Finally, electric field gradients (EFG) and quadrupolar tensors (Q) were computed at the PBE[48] level using the ADF code.[52,53] In this case, an all-electron triple-ζ valence plus polarization STO basis set (TZVP in ADF notation) was used for all atoms. This level of theory was already validated by previous studies on similar compounds.[52] The optimized structure of VOTPP is shown in Figure 1, with indication of the different types of hydrogen and carbon nuclei which can be detected by ENDOR and HYSCORE. The calculated directions of the dipolar and quadrupolar tensor axes of ^{14}N are also represented. One axis is parallel to the V═O bond, and another is parallel to the V−N bond.

Results

Structure of Vanadyl−Porphyrin Trapped in Silica. ***Continuous-Wave EPR.*** A typical cw-EPR spectrum at room temperature of VOTPP encapsulated in silica (VOTPP−SiO_2 sample) is represented in Figure 2. An identical spectrum (not shown) is obtained when VOTPP is encapsulated with BSA in silica (VOTPP/BSA−SiO_2 sample), which is an indication that vanadyl−porphyrins are not perturbed by the presence of biomacromolecules in silica. In addition, we observed no EPR spectrum when only BSA was encapsulated (BSA−SiO_2 sample), showing that the intense line in the middle of the spectrum is not due to organic radicals or defects of the SiO_2 matrix but represents the orientation-independent $m_I = -1/2$ vanadium hf line. The shape of the spectrum, characterized by narrow hf lines at room temperature, is identical to that of VOTPP in frozen solution at low temperature,[54] which shows that VOTTP is immobilized in silica cages, avoiding tumbling motion. The magnetic parameters deduced from simulation of the spectrum (Figure 2 and Table 1) are very close to those found for VOTPP in frozen solution, which confirms that the four-fold symmetry of the complex is conserved in SiO_2 and that despite its immobilization, the vanadyl−porphyrin complex is not perturbed by the mineral matrix. Consequently, VOTPP is easily trapped in a SiO_2 matrix, and it appears likely that vanadyl−porphyrin complexes with porphyrin moieties originating from primitive microorganisms could have fossilized in SiO_2 sediments of ancient seas.

^{1}H-ENDOR Spectroscopy. Proton ENDOR spectroscopy was used to probe in detail the effect of confinement of the porphyrin

TABLE 1: Spin Hamiltonian Parameters of Vanadyl in Synthetic VOTPP−SiO_2 Samples and in the 3490 Myr Old Dresser Chert[a]

sample	VO^{2+} species	g factors	hf parameters (10^{-4} cm^{-1})	localization and structure
VOTPP in SiO_2	VOTPP	$g_{\|\|} = 1.9655 \pm 0.0005$ $g_\perp = 1.984 \pm 0.003$	$A_{\|\|} = 154$ $A_\perp = 52$	Undistorted VOTPP encapsulated in SiO_2
	V1′	$g_{\|\|} = 1.938 \pm 0.003$ $g_\perp = 1.976 \pm 0.004$	$A_{\|\|} = 175$ $A_\perp = 63$	VO^{2+} bonded to four oxygen atoms of SiO_2
3490 Myr old chert	V1	$g_z = 1.941 \pm 0.002$ $g_x = 1.970 \pm 0.005$ $g_y = 1.997 \pm 0.005$	$A_z = 167$ $A_x = 61 \pm 2$ $A_y = 62 \pm 2$	VO^{2+} bonded to four oxygen atoms of the SiO_2 matrix

[a] Hyperfine (hf) parameters correspond to ^{51}V coupling.

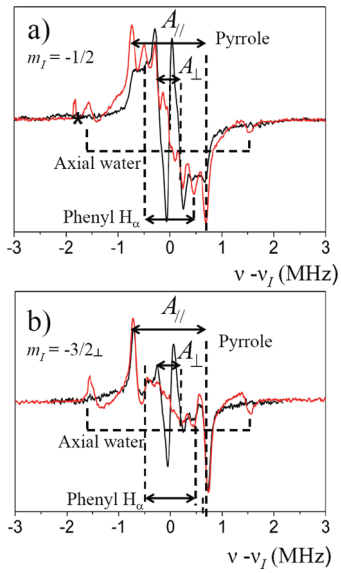

Figure 3. ^{1}H-ENDOR spectra at 10 K of VOTPP−SiO_2 (black) and VOTPP in frozen $CHCl_3$ solution (red). Microwave power: 6 mW; radio frequency power: 100 W; modulation frequency 25 kHz; modulation depth: 50 kHz. (a) Field setting $m_I = -1/2$; (b) field setting $m_I = -3/2_\perp$

complex in the SiO_2 matrix by comparing the proton hf parameters of VOTPP−SiO_2 with those of VOTPP diluted in frozen $CHCl_3$ solution, where interactions between metal complexes and the solvent cages are negligible,[55,56] and with hf parameters predicted from DFT calculation on VOTPP in vacuum. The vanadium hf transitions used as observers for ENDOR and HYSCORE spectroscopies are indicated by arrows in Figure 2. The central hf line ($m_I = -1/2$) is the most intense because its position is independent of the orientation of the magnetic field $\mathbf{B}_0$ with respect to the V=O bond (which defines the z-axis of the g factor and the vanadium hf interaction). There is no selection of molecular orientation with this field setting, and the ENDOR signal-to-noise ratio is optimized in this case. On the contrary, only VOTPP complexes with V=O oriented perpendicular and nearly parallel to $\mathbf{B}_0$ can be selected by setting the observing field at the $m_I = -3/2_\perp$ and $-7/2_{||}$ positions, respectively (Figure 2). However, it was not possible to use the $-7/2$ parallel field setting because of the very low ENDOR intensity in this case, resulting from the relatively weak ENDOR enhancement found for VOTPP in SiO_2.

Figure 3 compares ^{1}H-ENDOR spectra at 10 K of VOTPP−SiO_2 (in black) and VOTPP in frozen $CHCl_3$ solution (in red) for the field settings $m_I = -1/2$ and $-3/2_\perp$. The experimental and DFT-computed hf parameters are given in Table 2, and the corresponding hydrogen positions in the complex are shown in Figure 1. Classically, small proton hyperfine interactions are characterized by the Fermi contact term a_{iso} and the dipolar interaction T

$$A(\theta) = a_{iso} + T(3\cos^2\theta - 1) \quad (2)$$

with θ as the angle between the external field $\mathbf{B}_0$ and the electron−proton vector. For vanadyl complexes in a disordered medium, corresponding to the "weak coupling" situation ($|A| < 2\nu_I$, with $\nu_I = 14.4$ MHz at 340 mT for ^{1}H), each type of proton exhibits two pairs of ENDOR turning points corresponding to the orientation $\theta = 0$ and 90° at frequencies

$$\begin{aligned} \nu_{||}^{\pm} &= |\nu_I \pm A_{||}/2| \\ \nu_{\perp}^{\pm} &= |\nu_I \pm A_{\perp}/2| \end{aligned} \quad (3)$$

where signs + and − correspond to m_s states +1/2 and −1/2, respectively. DFT calculations predict that pyrrole hydrogen nuclei (H_{pyr} in Figure 1) exhibit the dominant hf interaction, with $A_{||} = +1.38$ MHz and $A_\perp = -0.36$ MHz, followed by phenyl hydrogen in the ortho position (H_o in Figure 1), with $A_{||} = +0.98$ MHz and $A_\perp = -0.46$ MHz. The analysis of ENDOR spectra is easier with the field setting $m_I = -3/2_\perp$ (Figure 3b), which selects VOTPP complexes with $\mathbf{B}_0$ lying in the porphyrin plane and gives a better resolution than without orientation selection (field setting $m_I = -1/2$, Figure 3a). The doublet characterized by $A = 1.38$ MHz corresponds clearly to $A_{||}$ of pyrrole protons. It is worth noticing that the same values are found for VOTPP in silica and in frozen solution. This is a further indication that the confinement in the silica matrix does not perturb the vanadyl−porphyrin interaction. The corresponding perpendicular hf interaction of the pyrrole protons is $A_\perp = -0.3$ MHz for VOTPP in silica. This component cannot be distinguished in the frozen solution with the field setting $m_I = -3/2_\perp$ (Figure 3b) because it interferes with the matrix ENDOR signal of $CHCl_3$. However the value $A_\perp = -0.3$ MHz for pyrrole hydrogen is measured both in silica and in frozen solution with the field setting $m_I = -1/2$ (Figure 3a). Thus, we may conclude that pyrrole protons H_{pyr} are characterized by the same hf parameters $a_{iso} = +0.26$ MHz and $T = +0.56$ MHz in the silica matrix and in frozen solution, which are also in good agreement with DFT calculation ($a_{iso} = +0.22$ MHz and $T = +0.58$ MHz) and with experimental values measured by Mulks and Van Willigen for VOTPP in frozen solution ($a_{iso} = +0.29$ MHz, $T = 0.55$ MHz).[54] Interaction with phenyl H_o protons (see Figure 1) is clearly observed with the field setting $m_I = -1/2$ only in the frozen solution ($A = 0.95 \pm 0.02$ MHz, Figure 3a). However, it is observed in both VOTPP−SiO_2 and VOTPP in frozen solution for the field setting $m_I = -3/2_\perp$ with the same coupling value $A = 0.98 \pm 0.02$ MHz (Figure 2b). These experimental values fully agree with the values $A_{||} = a_{iso} + 2T = +0.98$ MHz predicted by DFT for H_o phenyl protons (Table 2).

The only difference between VOTPP in SiO_2 and that in frozen $CHCl_3$ solution is the presence of an additional doublet with $A = 3.0(8)$ MHz for VOTPP in frozen solution. This

TABLE 2: Proton hf Interactions (in MHz) Calculated by DFT and Measured by ENDOR[a]

	pyrrole				phenyl					
	H_{pyr}		H_o		H_m		H_p		axial H_2O	
	a_{iso}	T	a_{iso}	T	a_{iso}	T	a_{iso}	T	a_{iso}	T
DFT	+0.2(2)	+0.5(8)	+0.02	+0.4(8)	0.00	+0.0(2)	0.00	+0.1(1)	+0.1	+4.5
VOTPP−SiO_2	+0.26	+0.56	~0.0	+0.47	nm	nm	nm	nm	absent	
VOTPP in $CHCl_3$	+0.26	+0.56	0.0	+0.47	nm	nm	nm	nm	3.08[b]	

[a] Experimental values for H_m and H_p protons are too weak to be measured (nm). [b] This value is obtained from DFT parameters for a V−O−H angle of 42°.

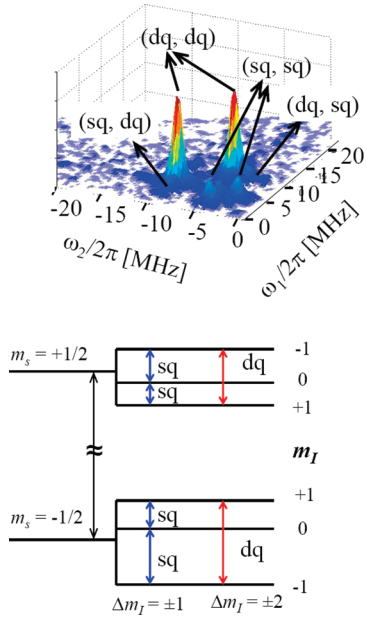

Figure 4. (top) 3D plot of the (+,−) quadrant HYSCORE at 4 K of VOTPP−SiO_2, recorded with the field setting $m_I = -7/2_{||}$, showing the main correlation peaks of ^{14}N. (bottom) Simplified energy level diagram for a $S = 1/2$, $I = 1$ system showing single quantum and double quantum transitions.

doublet is particularly intense with the field setting $m_I = -3/2_\perp$; however, it is lacking in the SiO_2 matrix. In their ENDOR study of VOTPP in frozen solution, Mulks and Van Willigen observed this doublet in pyridine but not in $CHCl_3$.[54] This variability indicates that it is most probably due to an axial water molecule impurity present in the solvent, forming a $H_2O\cdots V{=}O$ bond parallel to the C_4 axis. Our DFT calculations predict proton hf parameters $a_{iso} = +0.1$ MHz and $T = +4.5$ MHz for this axial water molecule (Table 2). A coupling of $A = 3.06$ MHz is calculated with these parameters for $\theta \approx 42°$ in eq 2, which is close to the mean angle value of $\langle\theta\rangle = 36°$ between the porphyrin plane and the V−H direction calculated by DFT for VOTPP in vacuum. Thus, an axial H_2O is likely at the origin of the proton hf interaction at 3.0(8) MHz in frozen $CHCl_3$ solution. The fact that it is lacking for VOTPP in SiO_2 simply indicates that such axial water molecules are always removed in the dry SiO_2 matrix.

A very weak ^{14}N ENDOR signal can be observed in the 2−6 MHz range. However, the poor ENDOR enhancement of VOTPP in SiO_2 and its decrease at low frequency indicate that cw-ENDOR is not well-adapted for ^{14}N study in this mineral host. For this reason, we used the methods based on nuclear modulation of electron spin echo.

^{14}N and ^{13}C HYSCORE Spectroscopy. Interactions with ^{14}N ($I = 1$, $\nu_I = 1.06$ MHz at 344 mT) and ^{13}C ($I = 1/2$, $\nu_I = 3.69$ MHz at 344 mT, 1.11% natural abundance) nuclei can be measured using HYSCORE spectroscopy, which is more adapted than ENDOR to nuclei with small magnetic moments and small hf interactions. In a HYSCORE experiment, characterized by the pulse sequence $\pi/2-\tau-\pi/2-t_1-\pi-t_2-\pi/2-\tau-$echo, the first part ($\pi/2-\tau-\pi/2$) of the sequence creates nuclear coherences (coherent superpositions of m_I states) in each $m_s = \pm 1/2$ state. The π pulse transfers each nuclear coherence from one m_s state to the other, and the last $\pi/2$ pulse transfers all nuclear coherences to the electron coherence (coherent superposition of $m_s = \pm 1/2$ states) for detection. A HYSCORE spectrum is obtained by recording the variation of the echo intensity upon stepwise variation of t_1 and t_2 delays before and after the π pulse, followed by Fourier transformation along t_1 and t_2. A two-dimensional frequency spectrum is obtained, with $\nu_1 = \omega_1/2\pi$ and $\nu_2 = \omega_2/2\pi$. The correlations between nuclear transitions appear as cross peaks in the 2D plot, which are distributed in two different quadrants (+,+) and (+,−) corresponding to $\omega_1 > 0$, $\omega_2 > 0$ and $\omega_1 > 0$, $\omega_2 < 0$, respectively. Nuclear modulations in the (+,+) quadrant correspond to the "weak coupling case" characterized by $|A| < 2|\nu_I|$, while the (+,−) quadrant corresponds to the "strong coupling case", with $|A| > 2|\nu_I|$. Typical HYSCORE spectra at 4 K are represented in Figures 4 and 5 for VOTPP−SiO_2 and show cross peaks and ridges in both quadrants.

All of the ^{14}N correlation peaks are localized in the (+,−) quadrant (strong coupling), while ^{13}C and ^{1}H correlations are localized in the (+,+) quadrant (weak coupling). The main characteristics of the ^{14}N spectrum are clearly observed in the 3D plot of the (+,−) quadrant, recorded with the field setting $m_I = -7/2_{||}$ (Figure 4a). This field setting corresponds to a single crystal-like orientation selection with $\mathbf{B}_0$ nearly parallel to the V=O axis. The interpretation of the cross peaks is given in the simplified energy level diagram shown in Figure 4b for an $S = 1/2$, $I = 1$ spin system. The spectrum is largely dominated by two sharp peaks corresponding to double quantum correlations (dq^+,dq^-) where the double quantum frequencies $\nu_{dq^\pm}$ (with + and − for $m_s = +1/2$ and $-1/2$, respectively) correspond to $\Delta m_I = \pm 2$ (Figure 4b). Their frequencies are given by[57,58]

$$\nu_{dq^\pm} = 2[(\nu_I \pm A/2)^2 + K^2(3 + \eta^2)]^{1/2} \qquad (4)$$

where $K = e^2Qq/4h$ is the quadrupole coupling constant and $\eta = (Q_{xx} - Q_{yy})/Q_{zz}$ is the asymmetry parameter, with Q_{xx}, Q_{yy}, and Q_{zz} being the three components of the quadrupolar interaction tensor. Two weaker correlation peaks at low frequency correspond to the single quantum correlations (sq^+,sq^-) corresponding to the selection rule $\Delta m_I = 1$. Other weak correlation peaks (sq^+,dq^-) and (dq^+,sq^-) can be seen in the flank of the sharp double quantum peaks (Figure 4a and Figure 5). All of the features are clearly observed on the contour plot representations of HYSCORE spectra shown in the top of Figure 5 for the $m_I = -7/2_{||}$ and $-3/2_\perp$ field setting conditions. The components of the hyperfine and the quadrupolar interactions of ^{14}N in VOTPP calculated by DFT are given in Table 3. They clearly correspond to the "strong coupling" situation. The spectra for $\tau = 128$ ns calculated with the DFT parameters are shown in the bottom of Figure 5. Although the general aspect of the spectrum is well-reproduced, it appears that the sharp double quantum peaks in the simulation appear at slightly higher frequencies than those in experimental spectra. This is due to a slight overestimate of the isotropic hf interaction by DFT calculation. The experimental parameters given in Table 3 are obtained from a direct measurement of the peak frequencies in the experimental spectra. Despite the small discrepancy for the isotropic a_{iso} interaction, the agreement between calculated and experimental parameters is very satisfying. The asymmetry parameter is however smaller with DFT ($\eta = 0.238$) than that in experimental spectra ($\eta = 0.58$). The experimental ^{14}N parameters for VOTPP−SiO_2 are also in good agreement with those previously obtained by Fukui et al. by ESEEM.[59] However, they are very different from those obtained by Mulks and Van Willigen by ENDOR,[54] VOTPP being in frozen solution in both cases (Table 3).

The (+,+) quadrant shows a proton peak at 14.6 MHz. The ridge crossing the diagonal $\omega_1 = \omega_2$ at the ^{13}C nuclear frequency

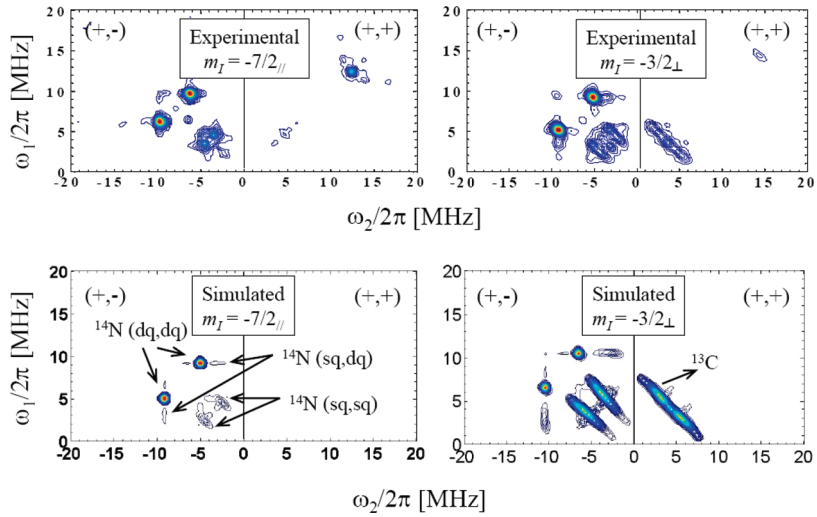

Figure 5. Experimental (top) and computed (bottom) HYSCORE spectra at 4 K of VOTPP−SiO_2 recorded by setting the magnetic field at the $m_I = -7/2_{||}$ (left) and $-3/2_{\perp}$ vanadium hf interactions; $\tau = 128$ ns. The pulse lengths are 16 and 32 ns for $\pi/2$ and π pulses, respectively. Simulations were performed with the same experimental parameters and with DFT-computed hf and quadrupolar parameters (corresponding to VOTPP in vacuum).

TABLE 3: Hyperfine and Quadrupolar Parameters (in MHz) of Pyrrole ^{14}N Calculated by DFT and Measured by HYSCORE in SiO_2 (this work) and by ENDOR and ESEEM in Frozen Solution by Other Authors[54,59]

sample	method	a_{iso}	T_{zz}//V=O	T_{xx}//V−N	T_{yy}	Q_{zz}//V−N	Q_{xx}//V=O	Q_{yy}	η
VOTPP in vacuum	DFT[a]	−8.27	− 0.66	+0.33	+0.33	+1.20	−0.45	−0.74	0.238
VOTPP−SiO_2	HYSCORE[a]	−7.5(5)	−0.6	+0.3	+0.3	+0.95	−0.2	−0.75	0.58
VOTPP in $CHCl_3$[b]	ENDOR[b]	−6.8	−1.21	−2.7	+3.89	±0.43	±0.26	±0.17	
VOTPP in CH_2Cl_2/toluene	ESEEM[c]	−7.3	−0.5	+0.5	0.0	+0.95	−0.20	−0.75	0.58

[a] This work. [b] Adapted from ref 54. [c] Adapted from ref 59.

TABLE 4: ^{13}C hyperfine Parameters (in MHz) Deduced from DFT Calculations

carbon	a_{iso}	T_{zz}	T_{xx}	T_{yy}
C_α	+5.10	+1.98	−1.20	−0.78
C_β	−0.59	+0.47	−0.28	−0.19
C_{brid}	−0.62	+1.13	−0.76	−0.37
C_{ph}	+0.40	+0.38	−0.21	−0.17
C_o	−0.07	+0.22	−0.12	−0.10
C_m	+0.01	+0.11	−0.06	−0.05
C_p	−0.005	+0.09	−0.05	−0.04

3.63 MHz, clearly observed with the field setting $m_I = -3/2_{\perp}$, is due to hf interactions with porphyrinic carbons. These modulations correspond to single quantum (sq) coherences, characterized by the selection rule $\Delta m_I = \pm 1$.[33] The ^{13}C hf parameters deduced from DFT calculation are given in Table 4. They are dominated by the interaction with carbon C_α of pyrrole groups (see Figure 1), followed by bridging carbons (C_{brid}). All other carbons exhibit smaller hf interactions. The ^{13}C HYSCORE spectrum calculated with DFT parameters at $\tau = 128$ ns (bottom right of Figure 5) reproduces fairly well the experimental spectrum (top right of Figure 5).

Thermal Stability of VOTPP in Silica. ***Continuous-Wave EPR.*** Thermal degradation of VOTPP encapsulated in SiO_2 was carried out in vacuum by isochronal heating treatments of the sealed tubes for short times (15 min) by steps of 50 °C and by recording the spectra at room temperature after each thermal step. We have previously shown that this experiment reproduces accurately the evolution of the EPR spectra of carbonaceous matter occurring during geologic evolution extending to more than 3000 million years.[60] The typical red color of VOTPP remains stable up to 320 °C and progressively turns to brown and then black at higher temperatures during carbonization

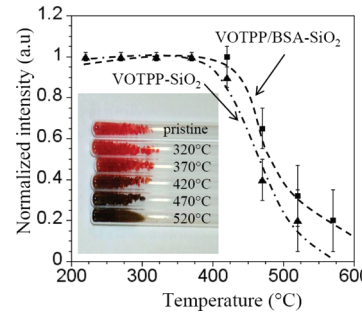

Figure 6. Evolution of the normalized EPR intensity of VO^{2+} in VOTPP−SiO_2 (full triangles) and VOTPP/BSA−SiO_2 (full squares) versus temperature of the step heating treatment. Discontinuous lines are guides for the eyes. Inset: color change of the material after each thermal step.

reaction (insert in Figure 6). The very good stability of VOTPP in SiO_2 is clearly shown by the intensity of the EPR spectra, which remains unchanged from room temperature to about 400 °C for VOTPP/BSA−SiO_2 and to about 350 °C for VOTPP−SiO_2 (Figure 6). The EPR intensity rapidly decreases for heating steps at higher temperatures, indicating a degradation of VOTPP as previously observed for VO−P in asphaltene and kerogen.[24] During this degradation, VO^{2+} are oxidized in diamagnetic V(V) species. It appears that the stability of VO^{2+} is slightly higher in VOTPP/BSA−SiO_2 than that in VOTPP−SiO_2 (Figures 6 and 7) as the latter completely vanished after a treatment at 570 °C while the former still showed a detectable EPR spectrum at this temperature (Figures 7 and 8). This improved stability can be explained by the reducing properties of the organic matter (BSA), which partially protects vanadyl against oxidation.[19]

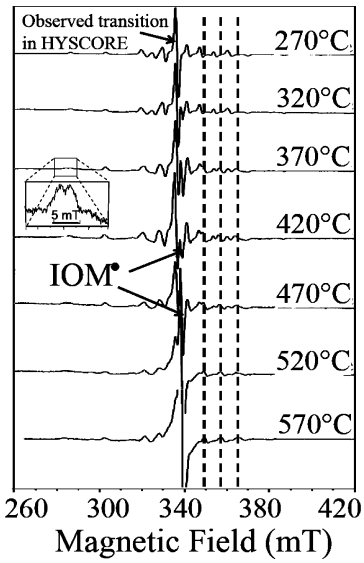

Figure 7. Evolution of the normalized EPR spectrum of VOTPP/BSA−SiO_2 upon step heating treatment. The insert represents the splitting of the $m_I = -7/2_{||}$ hf line at 370 °C. Vertical lines represent the position of some hf transitions of V1′ which appear at 370 °C.

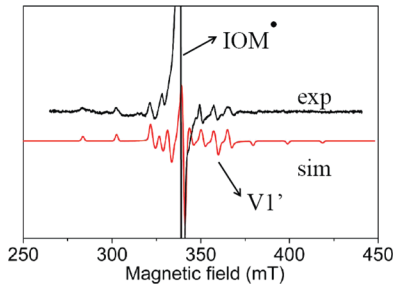

Figure 8. Experimental and simulated spectra of V1′ in VOTPP/BSA−SiO_2 after the heating step at 570 °C. The strong central line in the experimental spectrum is due to IOM• centers of the carbonaceous matter.

Figure 7 represents the evolution of the EPR spectrum of VOTPP/BSA−SiO_2 upon step thermal treatments. The spectrum is unchanged for treatments up to 320 °C. The intensity decreases by about 10% after the thermal step at 420 °C, and new EPR lines appear, which are more easily seen in the perpendicular hf pattern (marked by discontinuous lines) and by an apparent splitting of the $-7/2_{||}$ line (inset in Figure 7) due to a new V(IV) species, hereafter referred to as V1′, originating from the transformation of VOTPP. Also, a narrow EPR line at $g = 2.003$ appears in the flank of the central $-1/2$ hf line of vanadyl. This new line is due to paramagnetic defects (referred to as IOM• centers) of the carbonaceous matter (generally referred to as insoluble organic matter, IOM) produced by the thermal degradation of organic molecules and macromolecules.[60] This is confirmed by the fact that the IOM• line appears alone in the BSA−SiO_2 sample, which contains only encapsulated proteins (see inset in Figure 11). Upon increasing the step heating temperature, the total intensity of the VO^{2+} spectrum sharply decreases by oxidation, while the narrow line of IOM• centers increases. The remaining spectrum of VOTPP is progressively replaced by that of V1′, the replacement being almost completely achieved at 570 °C in the VOTPP/BSA−SiO_2 sample. At this stage, the new species V1′ contributes to about 10−20% of the initial VO^{2+} intensity. Its spectrum can be simulated (Figure 8) with the parameters given in Table 1.

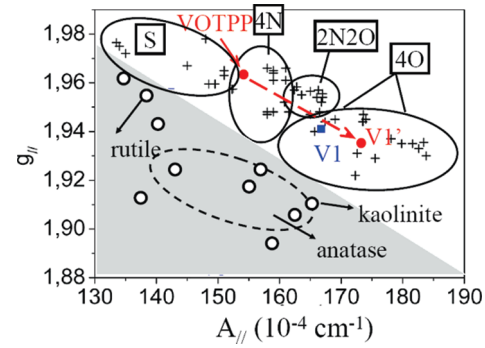

Figure 9. Plot of $g_{||}$ versus $A_{||}$ parameters for V(IV) in oxide minerals (○) and vanadyl VO^{2+} in oxides and in organic complexes (+). All of the data are taken from the literature.[35,61–75] The gray area corresponds to V(IV) in octahedral sites of the oxides. Data for minerals present in the chert; kaolinite, rutile, and anatase (inside of the area delimited by the discontinuous line) are highlighted. Data for VO^{2+} are located in the white area. The different ligand configurations (4O, 4N, 2N + 2O, 4S) of VO^{2+} are grouped in specific areas delimited by full lines. The blue square represent data for V1 species in the 3490 million year old chert from the Dresser formation, Warrawoona group, Western Australia. Data corresponding to VOTPP and V1′ in SiO_2 are represented by full circles (red).

It is well-known that parameters g and A are sensitive to the vanadium(IV) environment,[35] which allows us to determine the nature of the V1′ species. The most investigated type of V(IV) in the EPR literature is the vanadyl ion VO^{2+} with four ligands forming a square planar arrangement, which is the case with VOTPP. It has been shown that the hf constant of VO^{2+}, more particularly $A_{||}$ or the average value $\langle A \rangle = (A_{||} + 2A_{\perp})/3$, is correlated with the number and types of ligands in the equatorial plane.[61] In principle, this property can be used to interpret our spectra; however, it is valid only for VO^{2+}. Given that only parameters $g_{||}$ and $A_{||}$ can be accurately measured in our samples because the IOM• line obscures a broad part of the perpendicular hf pattern, we collected literature data for V(IV) with well-identified sites and ligands and plotted $A_{||}$ versus $g_{||}$ in Figure 9.[35,61–75] Black symbols represent the relation between $A_{||}$ and $g_{||}$ for VO^{2+} complexes (+ symbols) and V(IV) in oxides (open circles). Data for VO^{2+} (and V(IV) in oxides) are distributed outside (inside) of the gray area. The boundary between these two domains is approximate and is only a guide for the eyes. In the vanadyl domain, data for complexes with different types of ligands in the equatorial plane (4O, 4N, 2N2O, and S) are delimited in specific areas. Data for VOTPP and V1′ in SiO_2 are represented by red circles. It appears that V1′ is clearly localized in the domain of VO^{2+} in a square planar oxygen environment (Figure 9).

It is worth noticing that we always observed the simultaneous presence of two vanadyl species, namely, VOTPP and V1′, during the step thermal treatment of VOTPP encapsulated in SiO_2, with an increasing contribution of V1′ to the EPR spectrum upon increasing the heating temperature. This suggests that the destruction of VOTPP complexes proceeds via the transfer of VO^{2+} ion in an oxygenated environment, giving V1′ species, followed by the oxidation of V(IV) to V(V), and not by a progressive degradation of the porphyrin moiety in the VOTPP complex. In the latter case, we would expect a progressive destruction of the square planar nitrogen environment and a progressive replacement of N ligands by O ligands. Instead, in the course of the heating treatment, we always observed the association of unaffected VOTPP (four N ligands) and new VO^{2+} complexes with four O ligands (V1′), which points to a direct transfer of VO^{2+} from a porphyrin complex to a square

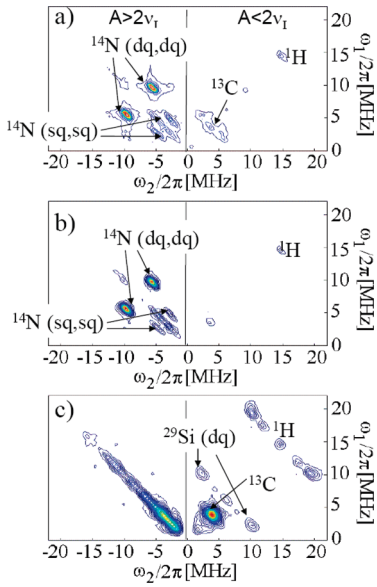

Figure 10. HYSCORE spectra at 4 K of (a) an untreated VOTPP/BSA−SiO_2 sample, (b) after thermal steps at 470 °C and (c) at 570 °C; τ = 128 ns; pulse lengths are 16 and 32 ns for $\pi/2$ and π pulses, respectively.

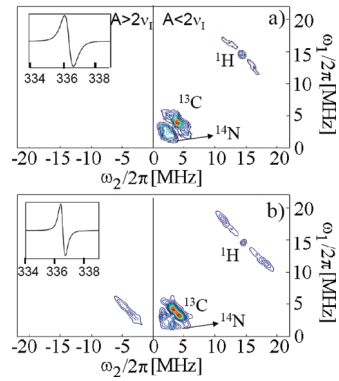

Figure 11. HYSCORE spectra at 4 K of a BSA−SiO_2 sample after thermal step at (a) 450 and (b) 550 °C; τ = 128 ns; pulse lengths are 16 and 32 ns for $\pi/2$ and π pulses, respectively. The corresponding cw-EPR spectra of IOM• centers formed during the degradation of BSA are shown in the insets.

planar oxygenated environment prior to the final oxidation of V(IV) to V(V). In their study of the stability of vanadyl−porphyrins in asphaltene/kerogen, Premovic et al.[24] showed that the degradation of these complexes is characterized by a broad range of activation energies, which agrees with our observation that the transformation of VOTPP into V1′ occurs along a broad temperature range.

In order to confirm this mechanism and to determine the nature of the V1′ complex, we used HYSCORE spectroscopy to identify the nearest-neighbor nuclei interacting with the VO^{2+} ion.

HYSCORE Spectroscopy. Selected HYSCORE spectra at 4 K of VOTPP/BSA−SiO_2, recorded before and after heating steps at 470 and 570 °C, are represented in Figure 10. For sensitivity reasons, the magnetic field was set at the intense $m_I = -1/2$ transition (see Figure 2). The pristine sample (Figure 10a) shows the same ^{14}N and ^{13}C correlation pattern as that with the $m_I = -3/2_\perp$ field setting (Figure 5). As anticipated by cw-EPR, there is no modification of the HYSCORE pattern upon heating steps at 270 and 320 °C. After heating steps at 370, 420, and 470 °C, the cw-EPR spectrum of VOTPP/BSA−SiO_2 contains both VOTPP and V1′ signals (Figure 7). The HYSCORE spectrum recorded after heating at 470 °C (Figure 10b) still shows sharp double quantum ^{14}N correlation peaks of the unaffected porphyrin ring. A progressive destruction of the porphyrin moiety would broaden the double quantum peaks by the distribution of hf and quadrupolar interactions induced by the disorder. However, it is clear that Figure 10b does not show any modification of the ^{14}N HYSCORE pattern. Furthermore, no additional signal can be attributed to the V1′ complex because the cw-EPR of the latter is too weak in this case to be observed in HYSCORE. The apparent lack of ^{13}C and ^{1}H peaks is the result of the lower cw-EPR intensity of VOTPP and organic radicals (IOM•) after the heating step at 470 °C. However, the HYSCORE spectrum of the sample containing only encapsulated BSA (BSA−SiO_2 sample) and heated at 450 °C (Figure 11a) clearly shows ^{1}H, ^{13}C, and ^{14}N peaks that are different from those of VOTPP. They represent hf interactions within organic radicals (IOM• centers) produced during thermal degradation of BSA. The corresponding cw-EPR lines of organic radicals are shown in the insets in Figure 11. It is interesting to note that ^{14}N-HYSCORE peaks of organic radicals appear in the (+,+) quadrant, corresponding to the "weak coupling" situation (Figure 11a). They correspond to N atoms of amide bonds of the protein, which have been incorporated in the IOM during carbonization.

After the heating step at 570 °C, the cw-EPR spectrum of VOTPP/BSA−SiO_2 shows only the V1′ complex and the intense line of organic radicals (IOM•) (Figures 7 and 8). In the (+,−) quadrant of the HYSCORE spectrum, ^{14}N (dq,dq) and (sq,dq) peaks of the porphyrin vanish and are replaced by an intense ridge along the diagonal $\omega_1 = \omega_2$. Such trace arises from antiphase echo due to strong dipole−dipole coupling and also to exchange interaction between electron spins. In the (+,+) quadrant, ^{1}H and ^{13}C peaks are mainly due to organic radicals (IOM•) resulting from the thermal degradation of BSA and TPP. This can be checked by comparing Figure 10c with Figure 11b representing the HYSCORE of BSA−SiO_2 recorded after the same heating treatment.

The important new feature of VOTPP/BSA−SiO_2 treated at 570 °C is that the (+,+) quadrant exhibits double quantum transitions of ^{29}Si centered at $2\nu_I$ = 5.82 MHz and peaking at 11.8−1.8 and 1.8−11.8 MHz (Figure 10c). These dq peaks are lacking in the BSA−SiO_2 sample after a similar heating (Figure 11b), which shows that they represent the hf interaction of the V1′ electron spin with ^{29}Si nuclei of the SiO_2 matrix. The single quantum ^{29}Si peaks around 2.9 MHz cannot be clearly observed because they overlap strongly with the broad ^{13}C pattern around 3.6 MHz. These double quantum ^{29}Si cross peaks can be attributed to the presence of equivalent silicon nuclei interacting with the vanadyl electron spin. Simulation of the cross-peak pattern gives the ^{29}Si hf parameters $A_x = -2.5$ MHz, $A_y = -2.7$ MHz, and $A_z = -3.8$ MHz. This vanadyl−silicon hf interaction is thus dominated by the isotropic Fermi contact term $a_{iso} = (1/3)(A_x + A_y + A_z) = -3.0$ MHz. Its amplitude and its negative sign (positive spin density on the silicon nucleus) indicates that the vanadium−silicon hf interaction occurs through a direct V···Si chemical bond,[76] reinforcing the interpretation according to which the oxygen atoms which coordinate VO^{2+} ions (V1′ species) belong to the SiO_2 matrix. The dipole−dipole term of the hf interaction, $T \approx (A_z - a_{iso})/2 = -0.4$ MHz is related to the V−Si distance r by $T = g\beta g_n\beta_n/r^3$, with the electron g factor $g = 2.003$, $g_n = -1.1106$ for ^{29}Si, and β and β_n being the electron and nuclear Bohr magnetons, respectively. The V−Si distance $r \approx 0.6$ nm is estimated from the hf interaction, which

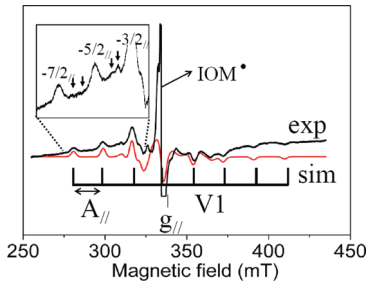

Figure 12. Experimental and simulated EPR spectra at 10 K of V1 species in the chert from the Dresser formation (3490 Myr). The stick diagram shows the parallel component of the ^{51}V hyperfine pattern. The intense central line is due to radicals of the insoluble organic matter (IOM• centers). The inset shows an expanded view of the low-field part of the spectrum. Very weak hf transitions of other V(IV) species are indicated by arrows. Microwave power, 1 mW; modulation amplitude, 0.5 mT.

again is compatible with the attribution of V1′ to a VO^{2+} ion coordinated to oxygen atoms of the SiO_2 network.

Vanadyl Ions in a 3490 Million Year Old Chert. To check the validity of our experimental approach, we studied by cw-EPR at 10 K a small piece of the Dresser chert, which contains some of the oldest putative traces of life on Earth (Figure 12). In addition to the intense line of paramagnetic centers of the insoluble organic matter (IOM• centers) common to all carbonaceous cherts,[60,77] the spectrum shows a hyperfine pattern typical of vanadium IV. Only the parallel set of ^{51}V hf lines is well-separated from other EPR signals in the chert and can be easily observed because $A_{||}$ is sufficiently large in that case. The perpendicular set with smaller hf splitting overlaps to some extent and is partially obscured by the strong line of IOM• centers and other paramagnetic centers.[60] The baseline is distorted by a very broad and weak ferromagnetic resonance signal of iron oxide particles. Also, other weak additional lines are present due to point defects in the SiO_2 matrix (E′ centers and $[AlO_4/h^+]$ centers for example).[60] The subtraction of this IOM line from the experimental spectrum was not possible because it exhibited an unusual stretched Lorentzian shape,[60] which has no analytical form.

The simulation (red line in Figure 12; Table 1) indicates that V(IV) lies in an environment with a nearly axial symmetry, the slight rhombicity improving the quality of the spectrum. It reproduces fairly well the spectrum, except the central part which contains other signals such as IOM• centers of the carbonaceous matter and point defects of SiO_2.[60] Neglecting the small rhombic distortion (Table 1), the parameters of V1 are characterized by $g_{||} = 1.941$, $g_{\perp} \approx 1.98$, $A_{||} = 18.4$ mT, and $A_{\perp} = 6.6$ mT. In the diagram of Figure 9, it appears that parameters of V1 correspond to the domain of VO^{2+} in a square planar oxygen environment and are close to that of V1′ resulting from the thermal degradation of VOTPP in SiO_2. By comparing the double integration of the simulated spectrum with that of the reference spectrum, the concentration of V1 (in spins by mass of chert) is estimated to $\sim 5 \times 10^{16}$ spin·g^{-1}. It must be emphasized that cherts are natural materials, and for this reason, they are intrinsically heterogeneous even at the scale of a millimeter size sample. We observed at least 100% variation of V1 intensity from sample to sample. The concentration estimated for the Dresser chert is the mean value obtained from five different samples taken in the same piece of rock.

Careful examination of the EPR spectrum shows that some very weak transitions occur between the $-7/2_{||}$ and $-3/2_{||}$ hf lines of V1 (insert in Figure 12). Their position (vertical arrows) and their splitting indicate that they are due to other V(IV) species in very low concentration. However, their very weak signals do not allow the evaluation of their magnetic parameters in pristine samples. In a work that will be published elsewhere, we show, by using a progressive demineralization of the SiO_2 matrix, that these additional lines are due to V(IV) impurities in minor mineral phases such as TiO_2 rutile and anatase.

It thus appears that the oxygenated VO^{2+} species V1′ and the paramagnetic defects of the carbonaceous matter (IOM• centers) resulting from the degradation of VOTPP in SiO_2 are very similar to the V1 species and the IOM• centers found in the Dresser chert that contains the most ancient putative traces of life. The small discrepancy of 0.9 mT (or 8.1×10^{-4} cm^{-1}) between the $A_{||}$ components of V1 and V1′ can be due to small differences in the degree of distortion of the equatorial oxygen ligands from a pure square planar configuration.[78]

Vanadyl as Potential Biomarkers of Primitive Life. From these results, it is tempting to attribute the oxygenated VO^{2+} complex found in the Archean chert (V1 species) to the ultimate degradation product of vanadyl−porphyrins (VO−P) trapped in the SiO_2 sediment 3490 Myr ago. As porphyrins are indisputably of biological origin, the demonstration of such filiations would be another argument in favor of a primitive life in the deposit environment of Dresser formation (3490 Ma), as recently proposed from molecular analysis.[29] However, three conditions are needed to validate this model; (1) the evolution of fossilized VO−P complexes in natural SiO_2 sediments for more than 3 billion years should be similar to the thermal degradation studied in the preceding section; (2) the conditions prevailing in the deposit environment of Dresser cherts should be favorable to the formation of VO−P complexes; and (3) even if oxygenated vanadyl complex V1 is actually a degradation product of vanadyl−porphyrins, it must be proven that these porphyrins are indigeneous to and synchronous with the SiO_2 host. In other words, it must be shown that the microorganisms at the origin of porphyrins are not the result of a later contamination by endolithic bacteria, for example.

It is difficult to demonstrate condition (1). However previous cw-EPR studies showed that various bituminous rocks, asphaltene, and asphalt containing VO−P give rise to oxygenated vanadyl complexes after heating at 150 and 250 °C for 1−20 days.[79] Also, the EPR spectra of these oxygenated VO^{2+} complexes are very close to those of nonporphyrin VO^{2+} compounds found in coals[79] and are very close to those of the V1′ complex of the present work, indicating similar structures of these complexes. Thus, the evolution from VO−P to oxygenated vanadyl complexes occurs also with geoporphyrins, which are known to be of biological origin. We can address now in more details the origin of vanadyl complexes in the 3490 Myr old chert of the Dresser formation. Concerning condition (2), analysis of the rare earth element composition and of the correlation between P, V, Zn, and Y with Fe indicate that the cherts of the Warrawoona Group (where the Dresser formation is located) are analogous to modern hydrothermal sediments deposited at mid-ocean ridges (MOR).[30] In addition, our samples contain well-crystallized barite microcrystals identified by their Raman spectrum (not shown), which indicates a relatively low-temperature deposition condition ($T \leq 100$ °C) near the hydrothermal vent.[30] The low-T hydrothermal SiO_2 sediments that deposited in this area may have thus fossilized organic matter and microorganisms in the presence of metal elements, such as vanadium, emanating from the hydrothermal vents. Vanadium is very soluble only in the V(V) state in the form of vanadate anions ($H_nVO_4^{n-3}$, $n = 0-4$). In anoxic water (which

was the case 3.5 billion years ago), biogenic and abiotic organic particles reduce vanadates and form vanadyl VO^{2+} that can be complexed with carboxylic acid moieties.[19] Thus, in the presence of biologic matter, vanadium should be initially present in the carbonaceous SiO_2 sediment in the form of oxygenated organic vanadyl complexes. However, these complexes cannot survive for long geological periods because carboxyl and hydroxyl ligands are eliminated during the first step of evolution of the biological matter (diagenesis).[19] Indeed, EPR study of various cherts with age between 2000 and 3500 Myr show that the IOM has lost all of its oxygenated ligands.[60] This means that the oxygenated vanadyl complex V1 of the Dresser chert cannot be the result of complexation with oxygenated functions of the IOM itself.

We now examine the possible role of biological porphyrins in the survival of oxygenated vanadyl complexes (V1 species of the chert). It is well-established that geoporphyrins exhibit an exceptional stability upon complexation with metal ions, mainly Ni(II) and VO^{2+}.[20] If porphyrins from bacteria were present in the sediment ~3500 Myr ago, vanadyl ions complexing the organic matter or adsorbed on mineral particles should have entered unmetalated porphyrins to form stable VO−P complexes.[18] These very stable complexes are found in sediments covering all Phanerozoic times (from present to 450 Myr).[21,22] However, we failed to detect such VO−P complexes in our 3490 Myr old chert samples by cw-EPR.

Consequently, taking into account the fact that (i) microorganisms and vanadium were present in the depositional environment of SiO_2 sediments of the Dresser formation[29,39] and (ii) that oxygenated vanadyl complexes similar to the V1 species of Dresser chert are likely the degradation products of geoporphyrins,[79] it appears that that the V1 species of the 3490 Myr old Dresser chert is most probably a degradation product of VO−P complexes originating from the presence of bacterial porphyrins. This hypothesis is reinforced by the present investigation of the thermal stability of VOTPP encapsulated in SiO_2, which shows that the degradation of VOTPP proceeds via a transfer of vanadyl to the oxygenated environment of the oxide matrix, forming an oxygenated VO^{2+} complex V1′ very similar to the V1 species of the Archean chert. The direct observation of V···Si interactions by HYSCORE spectroscopy of V1′ clearly demonstrates that the latter is localized in the SiO_2 matrix and not in the IOM itself. The V1 complex may thus be considered as ultimate relics of porphyrins from bacteria which lived in the vicinity of the hydrothermal vent 3490 Myr ago. Because porphyrins are found in all living systems, including most probably microorganisms that represented the early life on Earth, VO−P and oxovanadium complexes may also represent physicochemical markers of fossilized extraterrestrial life, in particular on Mars.[23]

However, it must be emphasized that oxygenated vanadyl can be considered as a potential biomarker for primitive life on Earth or Mars if $IOM^{\bullet}$ centers of carbonaceous matter (IOM) are also present. This is indeed the case with the Archean chert studied in this work (Figure 12) and experimentally verified with the thermal degradation of vanadyl−porphyrins encapsulated in silica. Consequently, the presence of vanadyl alone, without IOM in the rock, cannot be considered as a robust indication of their origin from vanadyl−porphyrins. Alternatively the presence of $IOM^{\bullet}$ centers alone is not a proof of the biological origin of the IOM preserved in the rock because it can be formed under abiotic conditions.[4−7] Indeed, abiotic IOM from carbonaceous meteorites exhibits EPR lines of $IOM^{\bullet}$ centers almost identical with those of Archean cherts.[80,81] Only the observation by HYSCORE of an excess of deuterium in $IOM^{\bullet}$ centers of meteorites provides a direct spectroscopic indication of their extraterrestrial origin.[82,83]

Conclusion

The structure, stability, and artificial aging of vanadyl−porphyrins trapped in sol−gel silica are studied by different EPR techniques assisted by DFT calculations. The evolution of the vanadyl environment and the associated paramagnetic defects are identical to those found in a ~3.5 billion years old microcrystalline SiO_2 rock (chert) containing the oldest traces of life on Earth. During their evolution, vanadyl ions of the porphyrin complexes are transferred to the silica host, giving oxygenated vanadyl complexes with square planar geometry. In addition, biomolecules and porpyrin moieties give an amorphous hydrogenated carbon material containing paramagnetic defects ($IOM^{\bullet}$ centers).

Acknowledgment. The authors acknowledge François Robert for providing chert samples and Region Ile-de-France for supporting the EPR facility. This work was supported by the program "Origin of planets and life" of Centre National de la Recherche Scientifique (CNRS) and by the Centre National d'Etudes spatiales (CNES).

References and Notes

(1) Southam, G.; Rothschild, L. J.; Westall, F. *Space Sci. Rev.* **2007**, *129*, 7–34.
(2) Schopf, W. J. *Science* **1993**, *260*, 640–645.
(3) Schopf, J. W.; Kudryavtsev, A. B.; Agresti, D. G.; Wdowiak, T. J.; Czaja, A. D. *Nature* **2002**, *416*, 73–76.
(4) Pasteris, J. D.; Wopenka, B. *Astrobiology* **2003**, *3*, 727–738.
(5) Brasier, M. D.; Green, O. R.; Jephcoat, A. P.; Kleppe, A. T.; Van Kranendonk, M. J.; Lindsay, J. F.; Steele, A.; Grassineau, N. V. *Nature* **2002**, *416*, 76–81.
(6) Brasier, M. D.; Green, O. R.; Lindsay, J. F.; McLoughlin, N.; Steele, A.; Stoakes, C. *Precambrian Res.* **2005**, *140*, 55–102.
(7) Garcia-Ruiz, J. M.; Hyde, S. T.; Carnerup, A. M.; Christy, A. G.; Van Kranendonk, M. J.; Welham, N. J. *Science* **2003**, *302*, 1194–1197.
(8) Mojzsis, S. J.; Arrhenius, G.; McKeegan, K. D.; Harrison, T. M.; Nutman, A. P.; Friend, C. R. L. *Nature* **1996**, *384*, 55–59.
(9) Schidlowski, M. *Precambrian Res.* **2001**, *106*, 117–134.
(10) Horita, J.; Berndt, M. F. *Science* **1999**, *285*, 1055–1057.
(11) Van Zuilen, M.; Lepland, A.; Arrhenius, G. *Nature* **2002**, *418*, 627–630.
(12) Mc Collom, T. M.; Seewald, J. S. *Earth Planet. Sci. Lett.* **2006**, *243*, 74–84.
(13) McKay, D. S.; Gibson Jr, E. K.; Thomas-Keprta, K. L.; Val, V.; Romanek, C. S.; Clemett, S. J.; Chillier, X. D. F.; Maechling, C. R.; Zare, R. N. *Science* **1996**, *273*, 924–930.
(14) Becker, L.; Glavin, D. P.; Bada, J. L. *Geochim. Cosmochim. Acta* **1997**, *61*, 475–481.
(15) Jull, A. J. T.; Courtney, C.; Jeffrey, D. A.; Beck, J. W. *Science* **1998**, *279*, 366–369.
(16) Madigan, M. T.; Martinko, J. M.; Parker, J. *Brock Biology of Microorganisms*; Prentice Hall: Upper Saddle River, NJ, 2003.
(17) Treibs, A. *Angew. Chem.* **1936**, *49*, 682–686.
(18) Larson, J. W.; Freeman, D. H. *Energy Fuels* **1990**, *6*, 627–748.
(19) Breit, G. N.; Wanty, R. B. *Chem. Geol.* **1991**, *91*, 83–97.
(20) Baker, E. W.; Louda, J. W. Thermal aspects of chlorophyll geochemistry. In *Advances in organic geochemistry*; Bjoroy, M., Ed.; John Wiley: London, 1983; pp 401−421.
(21) Serebrennikova, O. V.; Mozzhelina, T. K. *Org. Geochem.* **1994**, *21*, 891–895.
(22) Premovic, P. I.; Dordevic, D. M.; Pavlovic, M. S. *Fuel* **2002**, *81*, 2009–2016.
(23) Suo, Z.; Vuci, R.; Schweitzer, M. H.; Deliorman, M. *Astrobiology* **2007**, *7*, 605–615.
(24) Premovic, P. I.; Jovanovic, L. S.; Nikolic, G. S. *Org. Geochem.* **1996**, *24*, 801–814.
(25) Espinosa, M.; Campero, A.; Salcedo, R. *Inorg. Chem.* **2001**, *40*, 4543–4549.
(26) Walter, M. R.; Hofmann, H. J.; Schopf, J. W. In *Earth's earliest biosphere. Its origin and evolution*; Schopf, J. W., Ed.; Princeton University Press: Princeton, NJ, 1983; pp 385−413.

(27) Buick, R. *Palaios* **1990**, *5*, 441–459.
(28) Lowe, D. R. *Geology* **1994**, *22*, 387–390.
(29) Derenne, S.; Robert, F.; Skrzypczak-Bonduelle, A.; Gourier, D.; Binet, L.; Rouzaud, J. N. *Earth Planet Sci. Lett.* **2008**, *272*, 476–480.
(30) Kato, Y.; Nakamura, K. *Precambrian Res.* **2003**, *125*, 191–243.
(31) Feher, G. *Phys. Rev.* **1956**, 834–835.
(32) Höfer, P.; Grupp, A.; Nebenfürh, H.; Mehring, M. *Chem. Phys. Lett.* **1986**, *132*, 279–282.
(33) Schweiger, A.; Jeschke G. *Principle of pulsed electron paramagnetic resonance*; Oxford University Press, Oxford, U.K., 2001.
(34) Livage, J.; Coradin, T.; Roux, C. *J. Phys.: Condens. Matter* **2001**, *13*, R673–R691.
(35) Goodman, B. A.; Raynor, J. B. In *Electron spin resonance of transition metal complexes, Advances inorganic chemistry and radiochemistry*; Emeleus, H. J., Sharpe, A. G., Eds.; Academic Press: New York, 1970.
(36) Beaumont, V.; Robert, F. *Precambrian Res.* **1999**, *96*, 63–82.
(37) Dunlop, J. S. R.; Mui, M. D.; Milne, V. A.; Groves, D. I. *Nature* **1978**, *274*, 676–678.
(38) Awramik, S. M.; Schopf, J. W.; Walter, M. R. *Precambrian Res.* **1983**, *20*, 357–374.
(39) Van Kranendonk, M. J. *Earth Sci. Rev.* **2006**, *74*, 197–240.
(40) Stoll, S.; Schweiger, A. *J. Magn. Reson.* **2006**, *178*, 42–55.
(41) Frisch, M. J.; Trucks, G. W.; Schlegel, H. B.; Scuseria, G. E.; Robb, M. A.; Cheeseman, J. R.; Montgomery, J. A., Jr.; Vreven, T.; Kudin, K. N.; Burant, J. C.; Millam, J. M.; Iyengar, S. S.; Tomasi, J.; Barone, V.; Mennucci, B.; Cossi, M.; Scalmani, G.; Rega, N.; Petersson, G. A.; Nakatsuji, H.; Hada, M.; Ehara, M.; Toyota, K.; Fukuda, R.; Hasegawa, J.; Ishida, M.; Nakajima, T.; Honda, Y.; Kitao, O.; Nakai, H.; Klene, M.; Li, X.; Knox, J. E.; Hratchian, H. P.; Cross, J. B.; Bakken, V.; Adamo, C.; Jaramillo, J.; Gomperts, R.; Stratmann, R. E.; Yazyev, O.; Austin, A. J.; Cammi, R.; Pomelli, C.; Ochterski, J. W.; Ayala, P. Y.; Morokuma, K.; Voth, G. A.; Salvador, P.; Dannenberg, J. J.; Zakrzewski, V. G.; Dapprich, S.; Daniels, A. D.; Strain, M. C.; Farkas, O.; Malick, D. K.; Rabuck, A. D.; Raghavachari, K.; Foresman, J. B.; Ortiz, J. V.; Cui, Q.; Baboul, A. G.; Clifford, S.; Cioslowski, J.; Stefanov, B. B.; Liu, G.; Liashenko, A.; Piskorz, P.; Komaromi, I.; Martin, R. L.; Fox, D. J.; Keith, T.; Al-Laham, M. A.; Peng, C. Y.; Nanayakkara, A.; Challacombe, M.; Gill, P. M. W.; Johnson, B.; Chen, W.; Wong, M. W.; Gonzalez, C.; Pople, J. A. *Gaussian 03*, revision B.05; Gaussian, Inc.: Wallingford, CT, 2004.
(42) Adamo, C.; Barone, V. *J. Chem. Phys.* **1999**, *110*, 6158–6170.
(43) Neese, F. *Curr. Opin. Chem. Biol.* **2003**, *7*, 125–135.
(44) Saladino, A. C.; Larsen, S. C. *Catal. Today* **2005**, *105*, 122–133.
(45) Munzarova, M. L.; Kaupp, M. J. *J. Phys. Chem. B* **2001**, *105*, 12644–12652.
(46) Perdew, J. P.; Burke, K.; Ernzerhof, M. *Phys. Rev. Lett.* **1996**, *77*, 3865–3868.
(47) Adamo, C.; Barone, V. *Chem. Phys. Lett.* **1997**, *274*, 242–250.
(48) Dunning, T. H., Jr.; Hay, P. J. In *Modern Theoretical Chemistry*; Schaefer, H. F., III., Ed.; Plenum: New York, 1976; pp 1−28.
(49) Hay, J.; Wadt, W. R. *J. Chem. Phys.* **1985**, *82*, 299–310.
(50) Barone, V. In *Recent Advances in Density Functional Methods, Part I*; Chong, D. P., Ed.; World Scientific Publ. Co.: Singapore, 1995; pp 287−334.
(51) Rassolov, V.; Pople, J. A.; Ratner, M.; Windus, T. L. *J. Chem. Phys.* **1998**, *109*, 1223–1229.
(52) te Velde, G.; Bickelhaupt, F. M.; van Gisbergen, S. J. A.; Fonseca Guerra, C.; Baerends, E. J.; Snijders, J. G.; Ziegler, T. *J. Comput. Chem.* **2001**, *22*, 931–967.
(53) ADF2004.01, SCM, Theoretical Chemistry, Vrije Universiteit, Amsterdam, The Netherlands, http://www.scm.com (2004).
(54) Mulks, C. F.; van Willigen, H. *J. Phys. Chem.* **1981**, *85*, 1220–1224.
(55) Gourier, D.; Samuel, E.; Bachmann, B.; Hahn, F.; Heck, J. *Inorg. Chem.* **1992**, *31*, 86–95.
(56) Gourier, D.; Samuel, E. *J. Am. Chem. Soc.* **1987**, *109*, 4571–4578.
(57) Flanagan, H. L.; Singel, D. J. *J. Chem. Phys.* **1987**, *87*, 5606–5616.
(58) Maryasov, A. G.; Bowman, M. K. *J. Phys. Chem. B* **2004**, *108*, 9412–9420.
(59) Fukui, K.; Ohya-Nishiguchi, H.; Kamada, H. *J. Phys. Chem.* **1993**, *97*, 11858–11860.
(60) Skrzypczak-Bonduelle, A.; Binet, L.; Delpoux, O.; Vezin, H.; Derenne, S.; Robert, F.; Gourier, D. *Appl. Magn. Reson.* **2008**, *33*, 371–397.
(61) Chasteen N. D. EPR spin probes, inorganic and biochemical aspects. In *Biological Magnetic Resonance*; Berliner, L. J., Reuben, J., Eds.; Plenum Press: New York, 1981; pp 53−119.
(62) Kivelson, D.; Lee, S. K. *J. Chem. Phys.* **1964**, *41*, 1896–1903.
(63) Siegel, I. *Phys. Rev.* **1964**, *134*, 193–197.
(64) Assour, J. M.; Goldmacher, J.; Harrison, S. E. *J. Chem. Phys.* **1965**, *43*, 159–165.
(65) Barboux, P.; Gourier, D.; Livage, J. *Colloids Surf.* **1984**, *11*, 119–128.
(66) Che, M.; Canosa, B.; Gonzalezelipe, A. R. *J. Phys. Chem.* **1986**, *90*, 618–621.
(67) Cavani, F.; Centi, G.; Foresti, E.; Trifiro, F.; Busca, G. *J. Chem. Soc., Faraday Trans. 1* **1988**, *84*, 237–254.
(68) Centi, G.; Perathoner, S.; Trifiro, F.; Aboukais, A.; Aissi, C. F.; Guelton, M. *J. Phys. Chem.* **1992**, *96*, 2617–2629.
(69) Gehring, A. V.; Schosseler, P. M.; Weidler, P. G. *Geochim. Cosmochim. Acta* **1999**, *63*, 2061–2069.
(70) Luca, V.; McLachlan, D. J.; Bramley, R. *Phys. Chem. Chem. Phys.* **1999**, *1*, 2597–2606.
(71) Balikdjian, J. P.; Davidson, A.; Launay, S.; Eckert, H.; Che, M. *J. Phys. Chem. B* **2000**, *104*, 8931–8939.
(72) Tasiopoulos, A. J.; Troganis, A. N.; Deligiannakis, Y.; Evangelou, A. *J. Inorg. Biochem.* **2000**, *79*, 159–166.
(73) Kim, Y. J.; Kim, Y. I.; Choi, S. N. *Polyedron* **2000**, *19*, 2155–2161.
(74) Hwang, J. S.; Al-Turabi, M. O. H.; El-Sayed, L.; Al-Gwidi, H. A. M. *Energy Fuels* **2000**, *14*, 179–183.
(75) Cousin, R.; Capelle, S.; Abi-Aad, E.; Courcot, D.; Aboukais, A. *Chem. Mater.* **2001**, *13*, 3862–3870.
(76) Taylor, D. R.; Owen, J.; Wanklyn, B. M. *J. Phys. C: Solid State Phys.* **1973**, *6*, 2592–2610.
(77) Gourier, D.; Binet, L.; Skrzypczak, A.; Derenne, S.; Robert, F. *Spectrochim. Acta, Part A* **2004**, *60*, 1349–1357.
(78) Cornman, C. R.; Geiser-Bush, K. M.; Rowley, S. P.; Boyle, P. D. *Inorg. Chem.* **1997**, *36*, 6401–6408.
(79) Premovic, P. I.; Tonsa, I. R.; Pajovic, M. T.; Lopez, L.; Monaco, S. L.; Dordevic, D. M.; Pavlovic, M. S. *Fuel* **2001**, *80*, 635–639.
(80) Binet, L.; Gourier, D.; Derenne, S.; Robert, F. *Geochim. Cosmochim. Acta* **2002**, *66*, 4177–4186.
(81) Binet, L.; Gourier, D.; Derenne, S.; Robert, F.; Ciofini, I. *Geochim. Cosmochim. Acta* **2004**, *68*, 881–891.
(82) Gourier, D.; Robert, F.; Delpoux, O.; Binet, L.; Vezin, H.; Moissette, A.; Derenne, S. *Geochim. Cosmochim. Acta* **2008**, *72*, 1914–1923.
(83) Delpoux, O.; Gourier, D.; Binet, L.; Vezin, H.; Derenne, S.; Robert, F. *Spectrochim. Acta, Part A* **2008**, *69*, 1301–1310.

JP911728E